Few-Layer β-SnSe with Strong Visible Light Absorbance and Ultrahigh Carrier Mobility

Zhenqing Li,[1,2] Jin Li,[1,2,*] Chaoyu He,[1,2] Tao Ouyang,[1,2] Chunxiao Zhang,[1,2] Sifan Zhang,[1,2] Chao Tang,[1,2] Rudolf A. Römer,[3,2] and Jianxin Zhong[1,2,†]

[1] *Hunan Key Laboratory for Micro-Nano Energy Materials and Devices, Xiangtan University, Xiangtan, 411105 Hunan, China*

[2] *School of Physics and Optoelectronics, Xiangtan University, Xiangtan, 41115 Hunan, China*

[3] *Department of Physics, University of Warwick, Coventry CV4 8UW, United Kingdom*

(Received 29 September 2019; revised manuscript received 7 November 2019; published 23 January 2020)

Compared with traditional bulk materials, two-dimensional materials can exhibit exotic optoelectronic properties and especially provide large photoreactive contact areas, making them more attractive for designing alternative optoelectronic devices. In this work, we use first-principles methods based on density-functional theory to study the electronic and optical properties of few-layer β-SnSe. It is found that single-layer, double-layer, and triple-layer β-SnSe are semiconducting with direct band gaps of 1.38, 1.20, and 1.05 eV, respectively, which fall within the optimum band gap for solar cells. For triple-layer β-SnSe, the optical absorbance reaches 56% and the upper limit of the energy-conversion efficiency is 15.4%, which is comparable to the current efficiency record. Furthermore, few-layer β-SnSe has very high carrier mobility, reaching $10^7\ \mathrm{cm^2/V\,s}$ for triple-layer β-SnSe. The strong visible-light absorption and high carrier mobility of few-layer β-SnSe provide promising opportunities for applications in solar cells.

DOI: 10.1103/PhysRevApplied.13.014042

I. INTRODUCTION

Solar energy has enormous potential as a clean, abundant, and renewable energy source. The solar cell, which uses the photovoltaic effect to convert solar energy into electricity directly, has aroused widespread attention [1–4]. For solar-cell absorber and photovoltaic materials, the efficiency of visible-light adsorption is a critical factor for energy conversion and commercial applications. Solar cells based on silicon have high efficiency but high cost. A new generation of photovoltaic cells based on polymers and nanocrystalline semiconductor materials could provide some solutions for the more-economical production of such energy-conversion devices [5–8]. Compared with traditional bulk materials, two-dimensional (2D) materials can exhibit exotic optoelectronic properties far beyond those of their bulk counterparts and especially provide large photoreactive contact areas, making them more attractive for designing alternative optoelectronic devices [9–12]. Examples include phosphorene [13–16], graphitic carbon nitride [17–19], and monolayer transition-metal dichalcogenides [20–26] with desirable optoelectronic properties and large photoreactive contact areas for light absorption. In addition, several highly efficient 2D van der Waals heterojunction solar cells have been predicted theoretically and synthesized experimentally [27–32].

Similarly to transition-metal dichalcogenides, SnSe also crystallizes in a layered structure with weak bonding between the layers. SnSe has orthorhombic symmetry with space group *Pnma* at room temperature (α-SnSe), and has orthorhombic symmetry with space group *Cmcm* at high temperature (β-SnSe) (shown in Fig. 1). The phase transition from *Pnma* to *Cmcm* is of the second-order displacive type [33], which consists mainly of the continuous movement of Sn and Se atoms almost entirely along the [100] direction at a temperature of about 750–800 K [33,34]. SnSe was found to have a record high thermoelectric figure of merit at 923 K [34].

The low lattice thermal conductivity of β-SnSe due to anharmonic damping of low-frequency phonon modes has been investigated [35–37]. Exploiting the instability of electronic orbitals and lattice dynamics to generate strong anharmonicity may provide a new rationale to design efficient thermoelectric materials. In addition to the phase transition caused by high temperature, high-pressure-induced phase transitions of group-IV monochalcogenides were also widely studied [38–41].

*lijin@xtu.edu.cn
†jxzhong@xtu.edu.cn

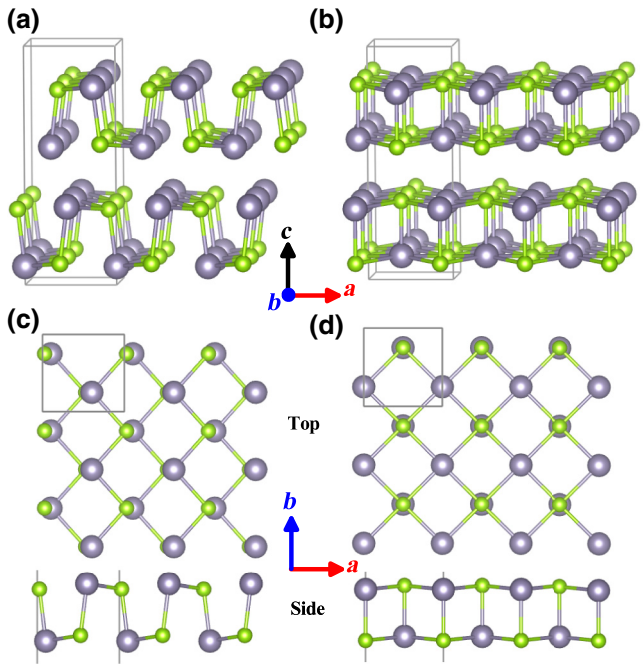

FIG. 1. Crystal structures of bulk (a) α-SnSe of space group *Pnma* (no. 62) and (b) β-SnSe of space group *Cmcm* (no. 63), and top and side views of (c) single-layer α-SnSe and (d) single-layer β-SnSe. The cuboid frames show the orthorhombic unit cells. Gray and green balls represent Sn and Se atoms, respectively.

As the counterpart of bulk α-SnSe, single-layer crystals of α-SnSe were prepared and investigated [42–47]. Nanocrystals of α-SnSe with a optimum band gap for solar cells and other advantages, such as Earth abundance, less toxicity, and chemical stability, have great potential for applications [45–47]. Shi *et al.* [44] studied the electronic and optical properties of single-layer, double-layer, and bulk α-SnSe and found that they exhibit unusually strong optical absorbance in the visible range. We noticed that although Baumgardner *et al.* [47] discovered that the hot-injection colloidal synthesis of SnSe nanocrystals could result in nanoparticles of both α-SnSe and β-SnSe, little known about nanocrystals of β-SnSe. In this work, we use first-principles methods based on density-functional theory to study the electronic and optical properties of few-layer SnSe in β-SnSe. It is found that single-layer, double-layer, and triple-layer β-SnSe are semiconducting with direct band gaps of 1.38, 1.20, and 1.05 eV, respectively. These results fall within the optimum band gap for solar cells. For triple-layer β-SnSe, the optical absorbance reaches 56% and the upper limit of the energy-conversion efficiency is 15.4%, which is comparable to the current efficiency record. Furthermore, few-layer β-SnSe has very high carrier mobility, reaching 10^7 cm^2/V s for triple-layer β-SnSe. The strong visible-light absorption and high carrier mobility of few-layer β-SnSe provide promising opportunities for applications in solar cells.

II. METHODS

Our first-principles calculations based on density-functional theory are performed with Vienna ab initio simulation package [48,49] with the Perdew-Burke-Ernzerhof (PBE) functional [50]. The interactions between the nucleus and valence electrons are described by the projector-augmented-wave method [51,52]. A plane-wave basis with a cutoff energy of 400 eV is used to expand the wave functions. The Brillouin-zone integration is obtained with $15 \times 15 \times 1$ and $6 \times 15 \times 15$ k-point grids for few-layer and bulk SnSe, respectively, following the scheme proposed by Monkhorst and Pack [53]. The convergence criteria for electronic and ionic relaxations are 10^{-6} eV and 10^{-3} eV/Å, respectively. For all models, van der Waals interactions are taken into account by the optB86b-vdW method [54–56]. For few-layer SnSe the vacuum regions are larger than 15 Å in the perpendicular direction to avoid interactions between them. The HSE06 functional is used for computation of electronic and optical properties [57]. Phonon band structures are calculated with the PHONOPY code [58], and ab initio molecular-dynamics simulations are used to examine the dynamical and thermal stability of the structures.

III. RESULTS AND DISCUSSION

The lattice parameters of α-SnSe and β-SnSe are calculated by PBE and the PBE functional corrected with optB88-vdW and optB86b-vdW. Table I presents the optimized lattice parameters and available experimental data for bulk α-SnSe and β-SnSe. As expected, the most-noticeable effects of considering the van der Waals interaction in the structural parameters are on the lattice vector perpendicular to the plane of the layers in the bulk. The results obtained with optB86b-vdW for the perpendicular lattice vector are closer to the experimental data for bulk β-SnSe. Hence, in the calculation, we use optB86b-vdW for few-layer β-SnSe.

TABLE I. Optimized lattice parameters (Å) for bulk and single-layer SnSe α and β phases obtained by the PBE, optB86b-vdW, and optB88-vdW methods. Experimental data are also listed [33].

		Bluk			Single layer	
		a	*b*	*c*	*a*	*b*
α-SnSe	PBE	4.43	4.18	11.58	4.38	4.28
	optB86b-vdW	4.41	4.19	11.60	4.30	4.27
	optB88-vdW	4.39	4.20	11.62	4.37	4.28
	Expt.	4.44	4.15	11.50		
β-SnSe	PBE	4.28	4.28	11.98	4.31	4.31
	optB86b-vdW	4.25	4.25	11.68	4.27	4.27
	optB88-vdW	4.30	4.28	11.91	4.31	4.31
	Expt.	4.31	4.31	11.70		

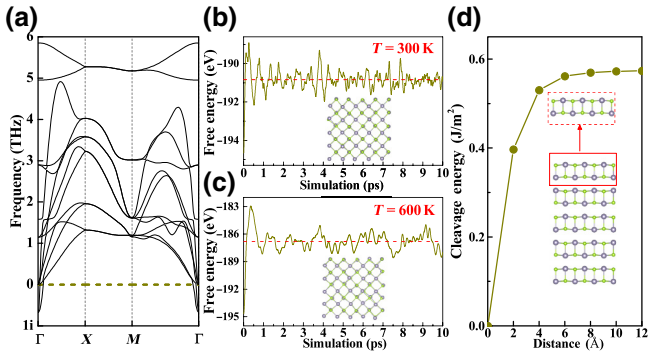

FIG. 2. (a) Phonon spectrum of single-layer β-SnSe. (b),(c) Total energy versus the simulation steps and final equilibrium structures (insets) at 300 and 600 K, respectively, for single-layer β-SnSe. (d) Cleavage energy as a function of separation distance for β-SnSe. The inset shows the separation of one layer from its neighboring four layers.

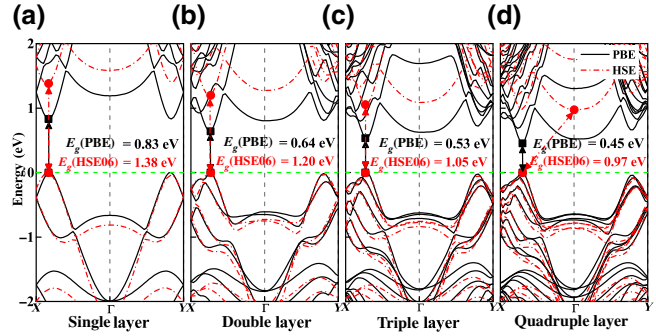

FIG. 3. Electronic band structures of (a) single-layer, (b) double-layer, (c) triple-layer, and (b) quadruple-layer β-SnSe. The Fermi level is shifted to the VBM.

We perform 10-ps ab initio molecular-dynamics calculations at 300 and 600 K with supercells of $3 \times 3 \times 1$ for single-layer β-SnSe to confirm its thermodynamic stability; the structures and energies are shown in Figs. 2(b) and 2(c). It is clear that thermal oscillations of atoms occur near their equilibrium positions, with no structural changes, indicating that single-layer β-SnSe has good thermodynamic stability. In addition, we calculate elastic constants for single-layer β-SnSe, and obtain $C_{11} = C_{22} = 49.54$ N/m, $C_{12} = 28.18$ N/m, and $C_{66} = 36.44$ N/m, which satisfy the mechanical stability criteria ($C_{11}C_{22} - C_{12}^2 > 0$ and $C_{66} > 0$) for the 2D material [59]. To estimate the dynamical stability of single-layer β-SnSe, we calculate the phonon band structure of single-layer β-SnSe, as shown in Fig. 2(a). The dispersion displays prominent imaginary modes around Γ, with the primary soft modes at the symmetry point. The phonon spectrum of bulk β-SnSe also has an imaginary frequency [35–37], but it can be prepared at a temperature about 750–800 K [33,34]. Compared with the bulk, few-layer β-SnSe appears more pervasively at lower temperatures (105 °C) [47]. On the other hand, high pressure can induce phase transitions of bulk group-IV monochalcogenides (SnS, GeS, and GeSe), which have a structure similar to that of SnSe, from the α phase to the β phase [38–41], and 2D α-SnSe has been synthesized by solution-phase synthesis [42,45–47] and vapor-phase synthesis [43]. So single-layer β-SnSe can be prepared at a certain temperature or strain.

For the layered bulk materials, mechanical cleavage [60] and liquid-phase exfoliation [61] are the most-popular techniques to produce single-layer and few-layer flakes. To assess the possibility of mechanical or liquid-phase exfoliation, we estimate the cleavage energy for cleavage of one layer from a five-layer slab serving as a model of the bulk. As shown in Fig. 2(d), when the distance between the exfoliating layer and its neighboring four layers is increased, the cleavage energy convergences at about $0.57\,\mathrm{J/m^2}$. For comparison, the experimentally estimated cleavage energy for cleavage of graphene from graphite is $0.37\,\mathrm{J/m^2}$ [62] and the estimated exfoliation energies calculated by density-functional theory for Ga_2N [63], (Na,Sn)P [64], GeP_3 [65], and GeS [66] are 1.09, 0.81, 1.14, and $0.52\,\mathrm{J/m^2}$, respectively. This indicates that it would be feasible to exfoliate single-layer and few-layer β-SnSe from bulk β-SnSe.

We calculate band structures of few-layer β-SnSe by first principles with the PBE and HSE06 functionals; the results are shown in Fig. 3. The band gap decreases with increasing number of layers; and the bulk band gap is 0.63 eV. Dingle-layer, double-layer, and triple-layer β-SnSe, have direct band gaps of 1.38, 1.20, and 1.05 eV, respectively, with the HSE06 functional, and the valence-band maximum (VBM) and conduction-band minimum (CBM) locates at Γ-X. When the CBM locates at Γ-X, the band structure is very steep around the CBM, leading to a very small effective mass (m^*/m_e) of about 0.1 for single-layer, double-layer, and triple-layer β-SnSe along the a direction. However, for quadruple-layer β-SnSe, the CBM locates at the Γ point with a very flat band structure around it, leading to an effective mass of about 1 along the a direction, which is nearly 10 times larger than the value for triple-layer β-SnSe. β-SnSe with more than three layers is an indirect-band-gap semiconductor, with its VBM locating at Γ-X and its CBM locating at the Γ point. All the band gaps of α-SnSe are indirect [44].

Considering the appropriate band-gap type and band-gap values, which fall within the optimum band gap for solar cells ($E_g = 1.0$–1.5 eV), we calculate the optical absorption of single-layer, double-layer, and triple-layer β-SnSe. We do not consider β-SnSe with four or more layers here because of the indirect band gap and large effective mass of the electron. The absorbance (A) of a 2D structure

as a function of photon energy E can be expressed as

$$A(E) = 1 - \exp\left(-\frac{E}{\hbar}\varepsilon_2 d\right), \tag{1}$$

where d is the simulation cell height in the perpendicular direction and ε_2 is the imaginary part of the dielectric function determined by a summation over empty states using the following equation [67] calculated by VIENNA AB INITIO SIMULATION PACKAGE:

$$\varepsilon^{(2)}_{\alpha\beta}(\omega) = \frac{4\pi^2 e^2}{\Omega} \lim_{q\to 0} \frac{1}{q^2} \sum_{c,v,k} 2\omega_k \delta(\varepsilon_{ck} - \varepsilon_{vk} - \omega) \times < u_{ck+e_{\alpha q}} | u_{vk} > < u_{vk} | u_{ck+e_{\beta q}} >, \tag{2}$$

where the indices c and v refer to conduction-band and valence-band states, respectively, and u_{ck} is the cell periodic part of the orbitals at the k point k.

As shown in Fig. 4, we find that the optical response of β-SnSe depends on the number of layers, but the optical responses along the a and b directions are almost the same. The optical absorbance reaches 26%, 45%, and 56% for single-layer, double-layer, and triple-layer β-SnSe, respectively, along the a direction. In particular, the optical absorbance of triple-layer β-SnSe is very high compared with other materials [23,25,44,68]. The combination of the unusually strong optical absorbance in the visible range and the ideal values of the direct band gap makes few-layer β-SnSe very promising for efficient ultrathin-photovoltaic applications.

On the basis of the overlap between the solar spectrum and the absorbance, we can estimate the upper limit of the converted power P [44]:

$$P = \frac{\int_0^{\lambda_{\max}} W(\lambda)A(\lambda)C(\lambda)d\lambda}{\int_0^{\infty} W(\lambda)d\lambda}, \tag{3}$$

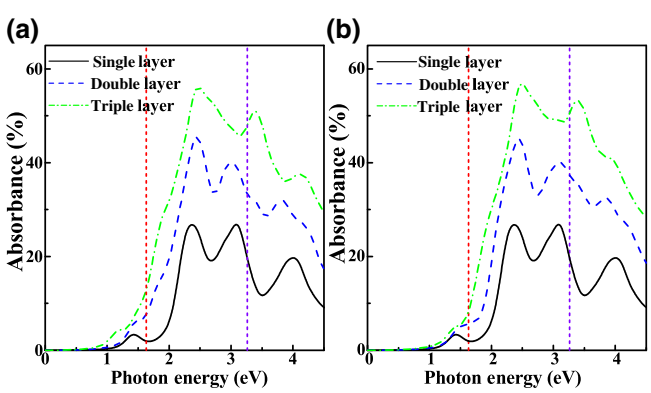

FIG. 4. Optical absorbance of few-layer β-SnSe along (a) the a direction and (b) the b direction. The area between the dashed red and purple lines represents the visible range.

TABLE II. Upper limit of the energy-conversion efficiency (%) for conversion of sunlight to the lowest-energy excitons for few-layer β-SnSe and α-SnSe along the a direction.

	Single layer	Double layer	Triple layer
β-SnSe	8.1	12.9	15.4
α-SnSe	7.7 (7.1 [44])	10.4 [44]	

where λ is the photon wavelength, $\lambda_{\max}$ is the longest wavelength that can be absorbed by few-layer β-SnSe determined by the lowest-exciton energy E_g of the minimum band gap of the material ($\lambda_{\max} = hc/E_g$), $W(\lambda)$ is the solar spectral irradiance at air mass 1.5 [69], $A(\lambda)$ is the directional absorbance of few-layer β-SnSe, and $C(\lambda)$ is the conversion factor to account for the fraction of the photon energy converted to the lowest-exciton energy [$C(\lambda) = \lambda(E_g/hc)$]. The upper limit of the energy-conversion efficiency for few-layer β-SnSe is given in Table II. Because of the great overlap between the solar spectrum and the absorbance, all the energy-conversion efficiencies of few-layer β-SnSe are considerable. The energy-conversion efficiency reaches 15.4% for triple-layer β-SnSe. This efficiency is comparable to the current efficiency record [44].

In addition to strong visible-light absorption, high carrier mobility is also important for highly efficient solar cells. To evaluate the carrier mobility (μ_{2D}), the widely used deformation-potential (DP) theory [70–74] proposed by Bardeen and Shockley [75] is used as

$$\mu_{2D} = \frac{e\hbar^3 C_{2D}}{k_B T m_e^* m_d (E_1^i)^2}, \tag{4}$$

where T, m_e^*, and m_d are room temperature (300 K), the effective mass, and the average effective mass determined by $m_d = \sqrt{m_x^* m_y^*}$, respectively. The DP constant E_1 for holes (electrons) can be determined as $E_1^i = \Delta V_i/(\Delta l/l_0)$, where ΔV_i is the energy change of the CBM (VBM) under uniaxial deformation along the transport direction, and l_0 and Δl are the corresponding lattice constant and deformation ratio. The elastic modulus C_{2D} of the longitudinal strain in the propagation direction (both x and y) of the longitudinal acoustic wave is derived from $(E - E_0/S_0) = C(\Delta l/l_0)^2/2$, where E is the total energy and S_0 is the equilibrium area of the system. Our calculations give only the upper bound of the carrier mobility because the DP theory considers only acoustic phonon scattering.

We evaluate the carrier mobilities of single-layer, double-layer, and triple-layer β-SnSe along the a and b directions shown in Fig. 1. We also calculate the carrier mobility of single-layer α-SnSe for comparison. The carrier mobilities and relevant parameters obtained with the HSE06 functional are listed in Table III. The calculated data for single-layer α-SnSe are of the same order

TABLE III. Carrier effective mass (m_e^*), elastic modulus (C_{2D}; J/m^2), deformation-potential constant (E_1; eV), and carrier mobility (μ_{2D}; 10^3 cm^2/V s) of single-layer, double-layer, and triple-layer β-SnSe and single-layer α-SnSe.

		a direction				*b* direction			
Carrier	System	m^*/m_e	C_{2D}	E_1	μ_{2D}	m^*/m_e	C_{2D}	E_1	μ_{2D}
Electron	Single layer (β)	0.14	50.19	0.88	70.43	0.14	50.19	0.88	70.43
	Double layer (β)	0.10	95.70	0.36	1379.34	0.13	101.30	7.32	2.716
	Triple layer (β)	0.09	139.75	0.14	17 785.52	0.12	149.71	6.67	5.75
	Single layer (α)	0.12	25.52	2.22	7.52	0.13	47.28	2.67	8.67
Hole	Single layer (β)	0.16	50.19	2.55	6.42	0.16	50.19	2.55	6.42
	Double layer (β)	0.11	95.70	2.86	21.60	0.10	101.30	7.64	3.70
	Triple layer (β)	0.10	139.75	2.43	50.41	0.10	149.71	4.94	13.07
	Single layer (α)	0.14	25.52	5.11	1.26	0.10	47.28	9.14	1.02

of magnitude as in a previous study [76]. By comparison we find that the electron mobility of single-layer β-SnSe is an order of magnitude greater than that of single-layer α-SnSe. From the calculations for single-layer α-SnSe and β-SnSe, we find that the difference in mobility is due to their different values of the elastic modulus (C_{2D}) and deformation-potential constant (E_1). By comparing the structures as shown in Figs. 1(c) and 1(d), we can see that single-layer α-SnSe is more prone to deformation than β-SnSe because it has longer bond lengths and greater spatial fluctuations. So single-layer α-SnSe has a smaller elastic modulus than β-SnSe along the *a* direction. On the other hand, the strong interaction results in large level splitting and a larger energy-level shift caused by strain, which leads to a larger deformation-potential constant as in black phosphorus [73]. From comparison of partial charge density at the VBM and CBM of single-layer α-SnSe and β-SnSe as shown in Fig. 5, we can see that α-SnSe has more charge distributed in the plane than β-SnSe, and the charge distribution of the Se and Sn atoms of β-SnSe is almost isolated. So α-SnSe has stronger interaction between Se and Sn atoms and a larger deformation-potential constant than β-SnSe.

Triple-layer β-SnSe has electron mobility of about 10^7 cm^2/V s along the *a* direction. Compared with other 2D materials that have been proposed to have high carrier mobility by the same method (i.e., the acoustic-phonon-limited scattering model in combination with the HSE06 functional), triple-layer β-SnSe has the highest carrier mobility. It is dozens of times higher than the theoretical value for grahene (3×10^5 cm^2/V s) [77], and almost hundreds of times higher than the highest value in black phosphorus (10^4 cm^2/V s) [78]. Such ultrahigh carrier mobilities arise mainly from the small effective mass of the electron and the small deformation potential. In addition to the ultrahigh mobility, the electron mobility is strongly anisotropic for double-layer and triple-layer β-SnSe.

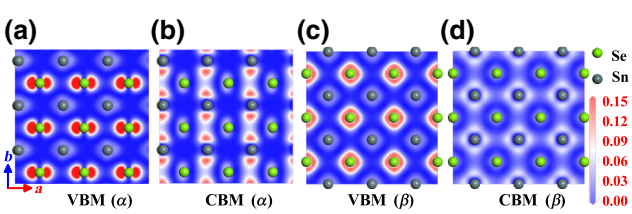

FIG. 5. Contour maps of partial charge density of single-layer α-SnSe at (a) the VBM and (b) the CBM and of β-SnSe at (c) the VBM and (d) the CBM in the plane.

IV. CONCLUSION

We use first-principles methods based on density-functional theory to study electronic and optical properties of few-layer β-SnSe. We find that single-layer, double-layer, and triple-layer β-SnSe are semiconducting with direct band gaps of 1.38, 1.20, and 1.05 eV, respectively, which fall within the optimum band gap for solar cells, leading to strong visible-light absorbance. For triple-layer β-SnSe, the optical absorbance reaches 56%, and the upper limit of the converted power is 15.4%. The steep band structures around the CBM lead to very small effective masses of about 0.1 along the *a* direction, which result in ultrahigh electron mobilities due to the small deformation-potential constants. Triple-layer β-SnSe has the highest electron mobility, of about 10^7 cm^2/V s along the *a* direction. Strong visible-light absorption and high carrier mobility are two critical factors affecting the application of solar cells. Our results suggest potential applications of few-layer β-SnSe in efficient, ultrathin, and flexible photovoltaic devices.

United Kingdom research data statement: all data accompanying this publication are directly available within the publication.

ACKNOWLEDGMENTS

This work was supported by the National Natural Science Foundation of China (Grants No. 11874316, No. 11974300, No. 11974299, No. 11704319, and No. 11404275), the National Basic Research Program of China (2015CB921103), the Program for Changjiang Scholars

and Innovative Research Team in University (Grant No. IRT13093), and the Furong Scholar Program of Hunan Provincial Government (R.A.R.).

[1] J. J. M. Halls, C. A. Walsh, N. C. Greenham, E. A. Marseglia, R. H. Friend, S. C. Moratti, and A. B. Holmes, Efficient photodiodes from interpenetrating polymer networks, Nature **376**, 498 (1995).

[2] S. E. Shaheen, C. J. Brabec, N. S. Sariciftci, F. Padinger, T. Fromherz, and J. C. Hummelen, 2.5% efficient organic plastic solar cells, Appl. Phys. Lett. **78**, 841 (2001).

[3] N. Armaroli and V. Balzani, The future of energy supply: Challenges and opportunities, Angew. Chem. Int. Ed. **46**, 52 (2007).

[4] B. E. Hardin, E. T. Hoke, P. B. Armstrong, J.-H. Yum, P. Comte, T. Torres, J. M. J. Fréchet, M. K. Nazeeruddin, M. Grätzel, and M. D. McGehee, Increased light harvesting in dye-sensitized solar cells with energy relay dyes, Nat. Photonics **3**, 406 (2009).

[5] W. U. Huynh, Hybrid nanorod-polymer solar cells, Science **295**, 2425 (2002).

[6] T. Watkins, A. V. G. Chizmeshya, L. Jiang, D. J. Smith, R. T. Beeler, G. Grzybowski, C. D. Poweleit, J. Menéndez, and J. Kouvetakis, Nanosynthesis routes to new tetrahedral crystalline solids: Silicon-like Si_3AlP, J. Am. Chem. Soc. **133**, 16212 (2011).

[7] G. Liu, P. Niu, L. Yin, and H.-M. Cheng, α-sulfur crystals as a visible-light-active photocatalyst, J. Am. Chem. Soc. **134**, 9070 (2012).

[8] J.-H. Yang, Y. Zhai, H. Liu, H. Xiang, X. Gong, and S.-H. Wei, Si_3AlP: A new promising material for solar cell absorber, J. Am. Chem. Soc. **134**, 12653 (2012).

[9] B. A. Gregg, The photoconversion mechanism of excitonic solar cells, MRS Bull. **30**, 20 (2005).

[10] D. Ginley, M. A. Green, and R. Collins, Solar energy conversion toward 1 terawatt, MRS Bull. **33**, 355 (2008).

[11] L. Li, Y. Yu, G. J. Ye, Q. Ge, X. Ou, H. Wu, D. Feng, X. H. Chen, and Y. Zhang, Black phosphorus field-effect transistors, Nat. Nanotechnol. **9**, 372 (2014).

[12] A. Molle, J. Goldberger, M. Houssa, Y. Xu, S.-C. Zhang, and D. Akinwande, Buckled two-dimensional Xene sheets, Nat. Mater. **16**, 163 (2017).

[13] R. R. Nair, P. Blake, A. N. Grigorenko, K. S. Novoselov, T. J. Booth, T. Stauber, N. M. R. Peres, and A. K. Geim, Fine structure constant defines visual transparency of graphene, Science **320**, 1308 (2008).

[14] X. Wang, L. Zhi, and K. Müllen, Transparent, conductive graphene electrodes for dye-sensitized solar cells, Nano Lett. **8**, 323 (2008).

[15] S. Bae, H. Kim, Y. Lee, X. Xu, J.-S. Park, Y. Zheng, J. Balakrishnan, T. Lei, H. R. Kim, Y. I. Song, Y.-J. Kim, K. S. Kim, B. Özyilmaz, J.-H. Ahn, B. H. Hong, and S. Iijima, Roll-to-roll production of 30-inch graphene films for transparent electrodes, Nat. Nanotechnol. **5**, 574 (2010).

[16] T.-H. Han, Y. Lee, M.-R. Choi, S.-H. Woo, S.-H. Bae, B. H. Hong, J.-H. Ahn, and T.-W. Lee, Extremely efficient flexible organic light-emitting diodes with modified graphene anode, Nat. Photonics **6**, 105 (2012).

[17] J. Zhang, X. Chen, K. Takanabe, K. Maeda, K. Domen, J. Epping, X. Fu, M. Antonietti, and X. Wang, Synthesis of a carbon nitride structure for visible-light catalysis by copolymerization, Angew. Chem. Int. Ed. **49**, 441 (2009).

[18] G. Liu, P. Niu, C. Sun, S. C. Smith, Z. Chen, G. Q. M. Lu, and H.-M. Cheng, Unique electronic structure induced high photoreactivity of sulfur-doped graphitic C_3N_4, J. Am. Chem. Soc. **132**, 11642 (2010).

[19] Y. Zhang and M. Antonietti, Photocurrent generation by polymeric carbon nitride solids: An initial step towards a novel photovoltaic system, Chem. Asian J. **5**, 1307 (2010).

[20] A. Splendiani, L. Sun, Y. Zhang, T. Li, J. Kim, C.-Y. Chim, G. Galli, and F. Wang, Emerging photoluminescence in monolayer MoS_2, Nano Lett. **10**, 1271 (2010).

[21] Q. H. Wang, K. Kalantar-Zadeh, A. Kis, J. N. Coleman, and M. S. Strano, Electronics and optoelectronics of two-dimensional transition metal dichalcogenides, Nat. Nanotechnol. **7**, 699 (2012).

[22] L. Britnell, R. M. Ribeiro, A. Eckmann, R. Jalil, B. D. Belle, A. Mishchenko, Y.-J. Kim, R. V. Gorbachev, T. Georgiou, S. V. Morozov, A. N. Grigorenko, A. K. Geim, C. Casiraghi, A. H. C. Neto, and K. S. Novoselov, Strong light-matter interactions in heterostructures of atomically thin films, Science **340**, 1311 (2013).

[23] M. Bernardi, M. Palummo, and J. C. Grossman, Extraordinary sunlight absorption and one nanometer thick photovoltaics using two-dimensional monolayer materials, Nano Lett. **13**, 3664 (2013).

[24] B. W. H. Baugher, H. O. H. Churchill, Y. Yang, and P. Jarillo-Herrero, Optoelectronic devices based on electrically tunable p-n diodes in a monolayer dichalcogenide, Nat. Nanotechnol. **9**, 262 (2014).

[25] A. Pospischil, M. M. Furchi, and T. Mueller, Solar-energy conversion and light emission in an atomic monolayer pn diode, Nat. Nanotechnol. **9**, 257 (2014).

[26] J. S. Ross, P. Klement, A. M. Jones, N. J. Ghimire, J. Yan, D. G. Mandrus, T. Taniguchi, K. Watanabe, K. Kitamura, W. Yao, D. H. Cobden, and X. Xu, Electrically tunable excitonic light-emitting diodes based on monolayer WSe_2 p-n junctions, Nat. Nanotechnol. **9**, 268 (2014).

[27] X. Duan, C. Wang, J. C. Shaw, R. Cheng, Y. Chen, H. Li, X. Wu, Y. Tang, Q. Zhang, A. Pan, J. Jiang, R. Yu, Y. Huang, and X. Duan, Lateral epitaxial growth of two-dimensional layered semiconductor heterojunctions, Nat. Nanotechnol. **9**, 1024 (2014).

[28] M. M. Furchi, A. Pospischil, F. Libisch, J. Burgdörfer, and T. Mueller, Photovoltaic effect in an electrically tunable van der waals heterojunction, Nano Lett. **14**, 4785 (2014).

[29] Y. Gong, J. Lin, X. Wang, G. Shi, S. Lei, Z. Lin, X. Zou, G. Ye, R. Vajtai, B. I. Yakobson, H. Terrones, M. Terrones, B. K. Tay, J. Lou, S. T. Pantelides, Z. Liu, W. Zhou, and P. M. Ajayan, Vertical and in-plane heterostructures from WS_2/MoS_2 monolayers, Nat. Mater. **13**, 1135 (2014).

[30] M. Shanmugam, R. Jacobs-Gedrim, E. S. Song, and B. Yu, Two-dimensional layered semiconductor/graphene heterostructures for solar photovoltaic applications, Nanoscale **6**, 12682 (2014).

[31] S. Wi, H. Kim, M. Chen, H. Nam, L. J. Guo, E. Meyhofer, and X. Liang, Enhancement of photovoltaic response in multilayer MoS_2 induced by plasma doping, ACS Nano **8**, 5270 (2014).

[32] Y. Gong, S. Lei, G. Ye, B. Li, Y. He, K. Keyshar, X. Zhang, Q. Wang, J. Lou, Z. Liu, R. Vajtai, W. Zhou, and P. M. Ajayan, Two-step growth of two-dimensional $WSe_2/MoSe_2$ heterostructures, Nano Lett. **15**, 6135 (2015).

[33] T. Chattopadhyay, J. Pannetier, and H. V. Schnering, Neutron diffraction study of the structural phase transition in SnS and SnSe, J. Phys. Chem. Solids **47**, 879 (1986).

[34] L.-D. Zhao, S.-H. Lo, Y. Zhang, H. Sun, G. Tan, C. Uher, C. Wolverton, V. P. Dravid, and M. G. Kanatzidis, Ultralow thermal conductivity and high thermoelectric figure of merit in SnSe crystals, Nature **508**, 373 (2014).

[35] C. W. Li, J. Hong, A. F. May, D. Bansal, S. Chi, T. Hong, G. Ehlers, and O. Delaire, Orbitally driven giant phonon anharmonicity in SnSe, Nat. Phys. **11**, 1063 (2015).

[36] J. M. Skelton, L. A. Burton, S. C. Parker, A. Walsh, C.-E. Kim, A. Soon, J. Buckeridge, A. A. Sokol, C. R. A. Catlow, A. Togo, and I. Tanaka, Anharmonicity in the HighTemperature Cmcm Phase of SnSe: Soft Modes and Three-Phonon Interactions, Phys. Rev. Lett. **117**, 075502 (2016).

[37] J. Hong and O. Delaire, Phase transition and anharmonicity in SnSe, Mater. Today Phys. **10**, 100093 (2019).

[38] H. C. Hsueh, H. Vass, S. J. Clark, G. J. Ackland, and J. Crain, High-pressure effects in the layered semiconductor germanium selenide, Phys. Rev. B **51**, 16750 (1995).

[39] S. Alptekin and M. Durandurdu, Formation of a Cmcm phase in SnS at high pressure; an ab initio constant pressure study, Solid State Commun. **150**, 870 (2010).

[40] M. Durandurdu, Cmcm phase of GeS at high pressure, Phys. Rev. B **72**, 144106 (2005).

[41] L. Ehm, K. Knorr, P. Dera, A. Krimmel, P. Bouvier, and M. Mezouar, Pressure-induced structural phase transition in the IV–VI semiconductor SnS, J. Phys.: Condens. Matter **16**, 3545 (2004).

[42] L. Li, Z. Chen, Y. Hu, X. Wang, T. Zhang, W. Chen, and Q. Wang, Single-layer single-crystalline SnSe nanosheets, J. Am. Chem. Soc. **135**, 1213 (2013).

[43] S. Zhao, H. Wang, Y. Zhou, L. Liao, Y. Jiang, X. Yang, G. Chen, M. Lin, Y. Wang, H. Peng, and Z. Liu, Controlled synthesis of single-crystal SnSe nanoplates, Nano Res. **8**, 288 (2015).

[44] G. Shi and E. Kioupakis, Anisotropic spin transport and strong visible-light absorbance in few-layer SnSe and GeSe, Nano Lett. **15**, 6926 (2015).

[45] M. A. Franzman, C. W. Schlenker, M. E. Thompson, and R. L. Brutchey, Solution-phase synthesis of SnSe nanocrystals for use in solar cells, J. Am. Chem. Soc. **132**, 4060 (2010).

[46] S. Liu, X. Guo, M. Li, W.-H. Zhang, X. Liu, and C. Li, Solution-phase synthesis and characterization of single-crystalline SnSe nanowires, Angew. Chem. Int. Ed. **50**, 12050 (2011).

[47] W. J. Baumgardner, J. J. Choi, Y.-F. Lim, and T. Hanrath, SnSe nanocrystals: Synthesis, structure, optical properties, and surface chemistry, J. Am. Chem. Soc. **132**, 9519 (2010).

[48] G. Kresse and J. Furthmüller, Efficiency of ab-initio total energy calculations for metals and semiconductors using a plane-wave basis set, Comput. Mater. Sci. **6**, 15 (1996).

[49] G. Kresse and J. Furthmüller, Efficient iterative schemes forab initiototal-energy calculations using a plane-wave basis set, Phys. Rev. B. **54**, 11169 (1996).

[50] J. P. Perdew, K. Burke, and M. Ernzerhof, Generalized Gradient Approximation Made Simple, Phys. Rev. Lett. **77**, 3865 (1996).

[51] P. E. Blöchl, Projector augmented-wave method, Phys. Rev. B. **50**, 17953 (1994).

[52] G. Kresse and D. Joubert, From ultrasoft pseudopotentials to the projector augmented-wave method, Phys. Rev. B. **59**, 1758 (1999).

[53] H. J. Monkhorst and J. D. Pack, Special points for brillouin-zone integrations, Phys. Rev. B. **13**, 5188 (1976).

[54] M. Dion, H. Rydberg, E. Schröder, D. C. Langreth, and B. I. Lundqvist, Van der Waals Density Functional for General Geometries, Phys. Rev. Lett. **92**, 246401 (2004).

[55] J. Klimeš, D. R. Bowler, and A. Michaelides, Chemical accuracy for the van der waals density functional, J. Phys.: Condens. Matter **22**, 022201 (2009).

[56] J. Klimeš, D. R. Bowler, and A. Michaelides, Van der waals density functionals applied to solids, Phys. Rev. B **83**, 195131 (2011).

[57] J. Paier, R. Hirschl, M. Marsman, and G. Kresse, The perdew–burke–Ernzerhof exchange-correlation functional applied to the G2-1 test set using a plane-wave basis set, J. Chem. Phys. **122**, 234102 (2005).

[58] D. Alfè, PHON: A program to calculate phonons using the small displacement method, Comput. Phys. Commun. **180**, 2622 (2009).

[59] Y. Ding and Y. Wang, Density functional theory study of the silicene-like siX and XSi3 (X = B, C, N, al, P) honeycomb lattices: The various buckled structures and versatile electronic properties, J. Phys. Chem. C **117**, 18266 (2013).

[60] K. S. Novoselov, D. Jiang, F. Schedin, T. J. Booth, V. V. Khotkevich, S. V. Morozov, and A. K. Geim, Two-dimensional atomic crystals, Proc. Natl. Acad. Sci. **102**, 10451 (2005).

[61] V. Nicolosi, M. Chhowalla, M. G. Kanatzidis, M. S. Strano, and J. N. Coleman, Liquid exfoliation of layered materials, Science **340**, 1226419 (2013).

[62] R. Zacharia, H. Ulbricht, and T. Hertel, Interlayer cohesive energy of graphite from thermal desorption of polyaromatic hydrocarbons, Phys. Rev. B **69**, 155406 (2004).

[63] S. Zhao, Z. Li, and J. Yang, Obtaining two-dimensional electron gas in free space without resorting to electron doping: An electride based design, J. Am. Chem. Soc. **136**, 13313 (2014).

[64] Y. Jiao, F. Ma, G. Gao, J. Bell, T. Frauenheim, and A. Du, Versatile single-layer sodium phosphidostannate(II): Strain-tunable electronic structure, excellent mechanical flexibility, and an ideal gap for photovoltaics, J. Phys. Chem. Lett. **6**, 2682 (2015).

[65] Y. Jing, Y. Ma, Y. Li, and T. Heine, GeP_3: A small indirect band gap 2D crystal with high carrier mobility and strong interlayer quantum confinement, Nano Lett. **17**, 1833 (2017).

[66] F. Li, X. Liu, Y. Wang, and Y. Li, Germanium monosulfide monolayer: A novel two-dimensional semiconductor with a high carrier mobility, J. Mater. Chem. C **4**, 2155 (2016).

[67] M. Gajdoš, K. Hummer, G. Kresse, J. Furthmüller, and F. Bechstedt, Linear optical properties in the projector-augmented wave methodology, Phys. Rev. B **73**, 045112 (2006).

[68] N. Luo, C. Wang, Z. Jiang, Y. Xu, X. Zou, and W. Duan, Saddle-point excitons and their extraordinary light absorption in 2D β-Phase group-IV monochalcogenides, Adv. Funct. Mater. **28**, 1804581 (2018).

[69] Tables for Reference Solar Spectral Irradiances: Direct Normal and Hemispherical on 37 Tilted Surface.

[70] S. Takagi, A. Toriumi, M. Iwase, and H. Tango, On the universality of inversion layer mobility in si MOSFET's: Part II-effects of surface orientation, IEEE Trans. Electron. Devices **41**, 2363 (1994).

[71] S. Bruzzone and G. Fiori, Ab-initio simulations of deformation potentials and electron mobility in chemically modified graphene and two-dimensional hexagonal boron-nitride, Appl. Phys. Lett. **99**, 222108 (2011).

[72] G. Fiori and G. Iannaccone, Multiscale modeling for graphene-based nanoscale transistors, Proc. IEEE **101**, 1653 (2013).

[73] J. Qiao, X. Kong, Z.-X. Hu, F. Yang, and W. Ji, High-mobility transport anisotropy and linear dichroism in few-layer black phosphorus, Nat. Commun. **5**, 4475 (2014).

[74] X. Shao, X. Liu, X. Zhao, J. Wang, X. Zhang, and M. Zhao, Electronic properties of a π-conjugated Cairo pentagonal lattice: Direct band gap, ultrahigh carrier mobility, and slanted Dirac cones, Phys. Rev. B **98**, 085437 (2018).

[75] J. Bardeen and W. Shockley, Deformation potentials and mobilities in non-polar crystals, Phys. Rev. **80**, 72 (1950).

[76] X. Li, X. Zuo, X. Jiang, D. Li, B. Cui, and D. Liu, Enhanced photocatalysis for water splitting in layered tin chalcogenides with high carrier mobility, Phys. Chem. Chem. Phys. **21**, 7559 (2019).

[77] J. Xi, M. Long, L. Tang, D. Wang, and Z. Shuai, First-principles prediction of charge mobility in carbon and organic nanomaterials, Nanoscale **4**, 4348 (2012).

[78] J. Xiao, M. Long, X. Zhang, J. Ouyang, H. Xu, and Y. Gao, Theoretical predictions on the electronic structure and charge carrier mobility in 2D Phosphorus sheets, Sci. Rep. **5**, 9961 (2015).